Automated Rapid Estimation of Flood Depth using Digital Elevation Model and EOS-04 Satellite derived flood inundation

Lakshmi Amani Chimata[1], Suresh Babu Anuvala Setty Venkata[1], Shashi Vardhan Reddy Patlolla[1], Durga Rao Korada Hari Venkata[1], Sreenivas Kandrika[1], Prakash Chauhan[1]

[1]National Remote Sensing Centre (NRSC), Indian Space Research Organization (ISRO), Hyderabad, India

Correspondence to: Lakshmi Amani Chimata (amanichimata@gmail.com)

Abstract. Rapid and accurate flood assessment is ~~essential~~crucial for effective ~~relief~~disaster response, rehabilitation, and ~~flood~~ mitigation strategies. ~~Developing and implementing automated, rapid methods for flood depth and inundation estimation are necessary for near real-time information dissemination.~~ This ~~paper~~study presents ~~an end-to-end,~~a fully automated ~~process~~framework for floodwater delineation and depth estimation using EOS-04 (RISAT-1A) Synthetic Aperture Radar (SAR) ~~images~~imagery and a Digital Elevation Model (DEM). ~~Flood inundation is estimated using an Automated~~This is the first study to apply the established Automatic Tile-~~based~~Based Segmentation ~~technique. Flood depth is estimated by~~ method and the Height above the Nearest Drainage (HAND) tool to EOS-04 data for flood extent delineation. For flood depth estimation, this study introduces a novel application of the Trend Surface Analysis (TSA) ~~method, a novel~~ technique ~~that requires only the inundated water layer~~, enabling rapid and ~~DEM, unlike various~~data-efficient assessment. Unlike traditional hydrodynamic models that ~~require~~demand extensive ~~data. This method~~ datasets and computational resources, TSA operates using only the inundated water layer and DEM, providing a highly data efficient solution.

The methodology is applied to ~~the most~~ flood-prone ~~areas~~regions in ~~the states of~~ Andhra Pradesh, Assam, Bihar, and Uttar Pradesh ~~in~~, India. ~~Water levels estimated at river gauge stations~~ Validation of flood extent against optical data demonstrates accuracy greater than 90%. Flood depth estimation using ~~the~~ TSA ~~technique are~~is validated by comparing water depths derived from river gauge stations with real-time field measurements and ~~compared with~~results from the Floodwater Depth Estimation Tool (FwDET~~) derived results. The TSA technique outperforms FwDET, showing lower~~). The TSA method achieves a root mean square error (RMSE~~ values.~~) of 0.805, significantly outperforming FwDET's RMSE of 5.23. This integration of high-resolution SAR imagery and DEM represents a transformative, automated solution for real-time flood monitoring and depth estimation, enhancing disaster management capabilities.

Key terms: Automation, Flood inundation, Flood depth

Formatted: Font: Not Bold

1 Introduction

Floods are frequent natural disasters that can have devastating consequences, including loss of life, destruction of property, and disruption of livelihoods. According to the National Disaster Management Authority (NDMA), India is highly susceptible to floods, with over 40 million hectares out of a total geographical area of 329 million hectares prone to flooding (https://ndma.gov.in/Natural-Hazards/Floods). A satellite-derived flood-affected area atlas (1998-2022) indicates that the flood-affected area in India is 15.8 million hectares, reflecting the impact of significant flood events and cyclones (https://ndma.gov.in/flood-hazard-atlases). However, satellite data may have limitations in capturing other flood-affected regions, such as flash floods of short duration and areas lacking satellite coverage during the flooding period. Certain rivers are critical, including the Brahmaputra and Barak in Assam, the Kosi and Ganga in Bihar, the Ganga and Yamuna in Uttar Pradesh, and the Godavari in Andhra Pradesh. ~~Additionally,~~Cyclone-prone states ~~frequently affected by cyclones,~~ such as Odisha, Andhra Pradesh, West Bengal, and Gujarat~~, have necessitated the preparation of Flood Hazard Zonation Atlases for these states, which~~ account for 10 million hectares of flood-affected areas~~ within these six states alone.~~, necessitating detailed hazard zonation maps. This highlights the ~~necessity~~critical need for real-time flood mapping and monitoring, the ~~adoption~~implementation of automated ~~techniques for~~ flood mapping techniques, and the generation of accurate spatial flood depth information to support disaster management efforts in these ~~areas~~regions.

Formatted: Line spacing: 1.5 lines, Pattern: Clear

~~The use of satellite~~Satellite data and ~~derived~~ flood inundation information ~~is popular~~are widely used for~~ addressing the~~ near real-time mapping and monitoring of flood events (Rizwan Sadiq et al., 2022). ~~and this needs to be performed with a reasonable level of confidence~~Accuracy in ~~respect of~~ flood ~~inundation areas, flood~~ extent and depth ~~which are~~is essential ~~in near real-time~~ for ~~enabling efficient~~effective relief ~~&~~and rehabilitation ~~activities~~efforts in the field~~ as the spatial information is aimed in this process~~. In this context, both Optical and Microwave satellite data sets are utilized, with the latter being more frequently used due to its advantage of satellite data acquisition under all weather conditions including rain, clouds, and sunlight, unlike sun-synchronous Optical satellite sensors (Felix Greifeneder et al., 2013). Therefore, space-borne Synthetic Aperture Radar (SAR) systems are preferred for flood monitoring. The techniques for ~~discussing~~ satellite-derived flood inundation mapping, flood depth estimation, and various case studies are examined from the literature~~ survey. Further~~. EOS-04, the ~~review underscores~~

~~the highlights of these studies,~~latest launch from ISRO, is designed to provide near real-time flood mapping and ~~the~~monitoring capabilities. Equipped with SAR sensors, it operates in both ascending and descending modes across coarse resolution mode (CRS), medium resolution mode (MRS) and fine resolution mode (FRS) configurations (A. V. Suresh Babu et al., 2024). The present research focuses on using newly launched EOS-404 satellite data to develop a methodology ~~and implementation~~ for automated, rapid estimation of ~~Flood Inundation Mapping and Flood Depth~~flood inundation mapping and flood depth estimation using the Digital Elevation Model.

SAR data uses unique properties of water to detect water covered areas. Generally, low backscatter measurements are possible in calm, open water surfaces with SAR data (Schlaffer et al., 2014). This property of SAR images makes distinguishing water from surrounding surfaces more effectively, even though visual interpretation helps flood mapping (Pierdicca et al. 2008). A literature survey revealed several articles on using SAR images for flood detection using various methods viz. (i) backscatter value-based thresholding (Boni et al., 2016, Chini et al., 2017, Greifeneder et al., 2014, Manjusree et al., 2012, Marti-Cardona et al., 2013, Martinis et al., 2015a, Martinis et al., 2013, Martinis et al., 2009, Twele et al., 2016), (ii) Interferometric coherence calculation (Chini et al., 2019), (iii) region growing and active contour model (Giustarini et al., 2013, Li et al., 2014, Matgen et al., 2011, Tong et al., 2018), (iv) object-oriented classification (Horritt et al., 2001, Kuenzer et al., 2013b, Mason et al., 2010, Pulvirenti et al., 2011), (iv) fuzzy classification (Martinis et al., 2015a, Twele et al., 2016), and (vi) change detection (Bazi et al., 2005, Giustarini et al., 2013, Martinis et al., 2011, Schlaffer et al., 2015, Shen et al., 2018). Among these methods, thresholding-based methods have been most widely used in the literature in part because they are computationally less time-consuming and meanwhile could yield comparable accuracy to the more complex segmentation approaches (Gstaiger et al., 2012; Kuenzer et al., 2013b). Among backscatter histogram thresholding algorithms, the OTSU method has been widely applied in image segmentation (Otsu 1979; Kittler and Illingworth 1986)). This method can automatically calculate the global threshold based on the criterion of maximum between-class variance and has high classification accuracy for images with a uniform bimodal distribution of gray histogram. However, suppose the histogram is unimodal or has non-uniform illumination, the traditional OTSU algorithm will fail and favour the class with a significant variance to improve the classification accuracy (Xu, X et al., 2011; Yuan et al., 2015). If the object size is less than 10% of the whole area, the performance of OTSU degrades significantly, and it will not be helpful for water detection methods (Cao et al., 2019).

Francesca et al., (2007) have used the method of dividing the SAR image into an unsupervised split-based approach (SBA) for change detection. This method automatically splits the image into a set of non-overlapping sub-images of user-defined size. Then, the sub-images are sorted according to their probability of containing many changed pixels. Afterward, a subset of splits with a high likelihood of containing changes is selected and analysed. This same change detection technique is applied for flood detection by Bovolo and Bruzzone (2007) to identify tsunami-induced changes in multi-temporal imagery~~.~~ and Martinis (2015) for flood mapping TerraSAR-X data. In view of the above limitation in the OTSU method and with the merits of the change detection method, the present study ~~proposed automated~~introduced a novel approach combining the OTSU threshold method with a tile-based segmentation strategy for flood extent delineation ~~of the flood mapping techniques using a Tile-based Segmentation technique i.e., Otsu's thresholding method along with a change detection approach~~in EOS-04 satellite.

However, there is a limitation to this technique when mapping in hilly areas. In very steep slopes, the hillside may appear completely dark, as no radar signal is returned at all, potentially leading to a false interpretation of water pixels. In addressing this issue, Giacomelli~~ et al.,~~ (1995) integrated a SAR image with a digital terrain model and employed a simple technique to exclude this false interpretation by utilizing slope, slope direction, and drainage information. Additionally, the Height Above the Nearest Drainage (HAND) tool has been used to exclude hilly areas, enhancing the efficiency of the extracted water layer output, as demonstrated by Nobre et al., (2011). In this approach, HAND raster values are appropriately classified to eliminate false interpretations in the water layer.

Formatted: Line spacing: 1.5 lines

In addition to the availability of flood inundation information in near real-time, it is crucial to have access to spatial flood depth maps for directing rescue and relief operations, pooling necessary resources, determining road closures and accessibility, and conducting post-event analysis (Islam et al., 2001). Flood depth identification during or after flood events is critical for assessing hazard levels and creating risk zone maps, which are essential for post-disaster flood mitigation planning. While direct surveying methods used to determine floodwater depth can be highly accurate, they are often influenced by weather conditions, costly, and may require field crews to obtain authorization to access sensitive flooded areas. In light of this, remote sensing-based techniques and digital elevation models (DEMs) are valuable for estimating flood depth (Ismail Elkhrachy et al., 2022). Various hydrodynamic models such as HEC-RAS, Delft-3D, and LISFLOOD-FP have been developed to simulate water levels and flood depths (Yalcin, 2018; Costabile et al., 2021). However, these models require extensive data inputs, such as rainfall, soil moisture, flood maps, gauge discharge, cross-sections, and other hydrological inputs, which result in significant computational time and resource requirements.

Formatted: Line spacing: 1.5 lines, Pattern: Clear

Cohen et al. (2007) developed a floodwater depth calculation model based on high-resolution flood extent and DEM layers, known as the FwDET (Flood Water Depth Estimation Tool). The FwDET model identifies the floodwater elevation for each cell within the flooded domain based on its nearest flood boundary grid cell. While FwDET has been evaluated as one of the ~~more~~most effective tools for estimating flood depth from remote sensing-derived water extent and DEM (Teng et al., 2022), it has inherent limitations. One critical limitation is that FwDET's floodwater depth maps are not continuous, often showing sharp transitions in values, which leads to linear stripes across the flooded domain~~. Additionally, FwDET's floodwater depth accuracy is poor in the case of active channels (Cohen et al., 2018). To overcome these limitations, this paper introduces a novel method called Trend Surface Analysis (TSA) to improve the accuracy of flood depth estimation. This method requires only a flood extent polygon and a DEM as input.~~ (Cohen et al., 2018).Trend surface analysis has long been used by geographers, geologists, and ecologists to fit surfaces to data recorded at sample points scattered across a two-dimensional sample space (Chorley et al., 1965).In this paper, flood depth is estimated using a novel application of Trend Surface Analysis, which utilizes only the inundated water layer and a Digital Elevation Model (DEM). This study introduces a novel approach for an end-to-end fully automated framework for floodwater delineation and depth estimation, utilizing real-time EOS-04 (RISAT-1A) Synthetic Aperture Radar (SAR) imagery and a Digital Elevation Model (DEM).

2. Study Area

The research focused on four significantly flood-affected regions in India's river plains: the Godavari, Brahmaputra, Kosi, and Ganga River basins. Table 1 provides detailed characteristics of flood proneness in these regions, while Figure 1 illustrates a location map and the input EOS-04 satellite images of the study areas.

Table 1: Study Area Locations and its characteristics

S.No	Location (Lat/Lon) -decimal degrees	State -Districts Covered, River Basin	Study Area (Sq.Km)	Characteristics of study area
1	17.4008°N to 17.8592°N and 80.9720°E to 81.6582°E	Andhra Pradesh-Alluri Sitaram Raju district	72km × 50km	Receives maximum rainfall during South West Monsoon. 84% of annual rainfall falls during the period starting in mid-June and ending by mid-October
2	25.9885°N to 26.7132°N and 90.6755°E to91.8661°E	Guwahati and Barpeta areas of Assam State	120km x 80km	The Brahmaputra River, known as, the lifeline of Assam, is one of the largest rivers in the world in terms of discharge
3	25.0975°N to 25.7142°N and 86.2874°E to 87.6618°E	Bhagalpur of Bihar State	138km x 68km	Floods frequently occur in Bihar over the Kosi river basin, hence the Kosi river is known as the "Sorrow of Bihar". Floods are generally caused by the breach of embankment along the Kosi river owing to intense rainfall during the monsoon season
4	27.0138°N to27.6943°~~N and 79~~Nand79.1919°E to80.1584°E	Farrukhabad area of Uttar Pradesh	95km x 75km	Vast majority of state lies within the Gangetic Plain. The weather is of tropical monsoon type

Formatted: Heading 3

Formatted: Justified, Indent: Left: 5.08 cm

Formatted Table

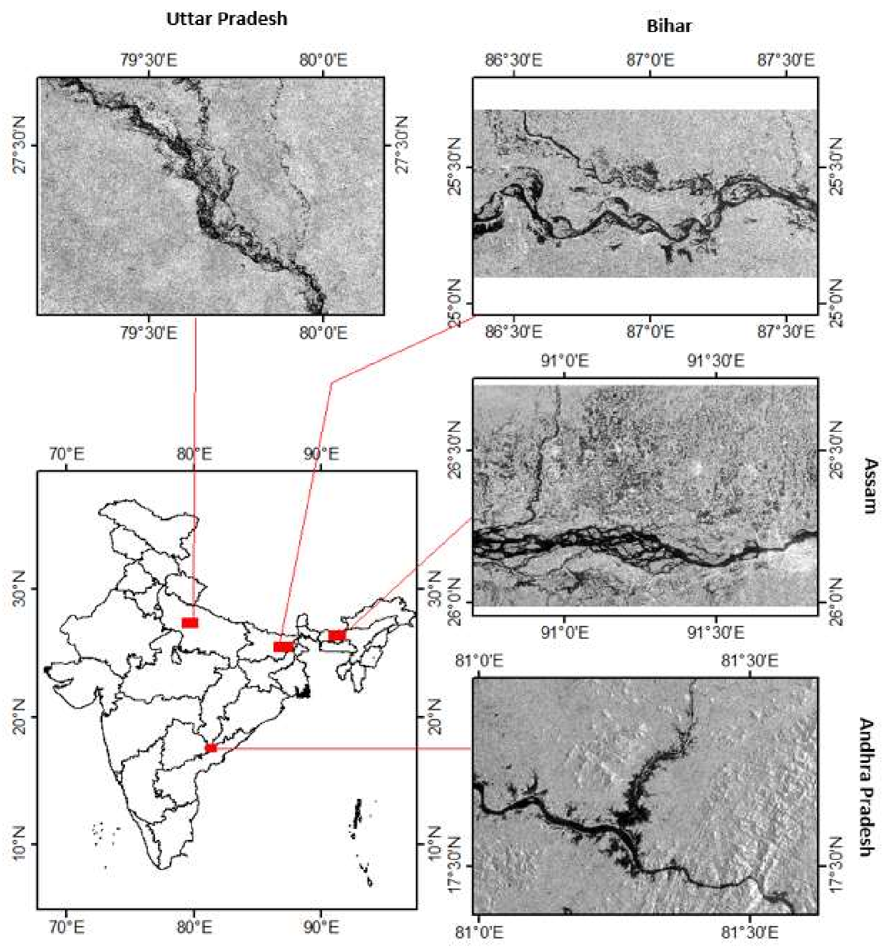

Figure.1. Map showing Four Study Area Locations: Andhra Pradesh, Assam, Bihar and Uttar Pradesh

3.~~ ~~Data used

~~Table 2~~Comprehensive details on the ~~information on Satellite~~satellite data and the associated Digital Elevation Model (DEM) ~~used~~utilized for ~~deriving Flood~~estimating flood inundation and depth ~~estimation.~~are provided in Table 2. To validate the flood extent layers, optical datasets were employed, with additional specifics outlined in Table 3. Figure 2 ~~provide~~illustrates the ~~Spatial~~ locations of ~~River~~river gauge stations ~~where~~and the field~~-~~-measured water levels ~~are~~ provided by the Central Water Commission (CWC) of India. In this figure 2, permanent water bodies within each study area are clearly highlighted in blue

Table.2. Satellite data and respective DEMs used for the flood extent and depth estimation

S.No	Study Area	Satellite Sensor	Satellite data Spatial Resolution(meters)	Satellite date and Time	~~DEM~~DEM used for the study area	DEM spatial Resolution (meters)
1.	Andhra Pradesh	EOS-04, CRS Mode	36	28th July 2023 at 18:00	LIDAR DEM	5
2.	Assam	EOS-04, CRS Mode	36	20thJune 2023 at 18:00	FAB - DEM COPERNICUS	30
3.	Bihar	EOS-04, MRS Mode	18	3rdSeptember 2023 at 06:00	FAB (Forest and Buildings removed) DEM COPERNICUS	30
4.	Uttar Pradesh	EOS-04, MRS Mode	18	15thAugust 2023 at 06:00	FAB-DEM COPERNICUS	30

Formatted Table

Table.~~2. Satellite data, DEMs~~**3**. Optical Data used for ~~the study~~Validation of flood extent

S.No	Study Area	Optical Dataset	Satellite data Spatial Resolution(meters)	Satellite date
1.	Bihar	Resourcesat-2 LISS-4 sensor	5.8m	3rdSeptember 2023
2.	Uttar Pradesh	Landsat-8	15m	15thAugust 2023

Formatted: Justified

3.1. Satellite Data digital elevation models

The Earth Observation Satellite-04 (EOS-04) is a synthetic aperture radar (SAR) satellite operating in the C-band frequency range of 5.4 GHz. Positioned in a sun-synchronous orbit at an altitude of 524.87 km, it offers various imaging modes, including Fine Resolution Strip ~~Map~~ Mode~~-1~~ (FRS~~-1), Fine Resolution Strip Map Mode-2 (FRS-2~~), Medium Resolution ScanSAR Mode (MRS), Coarse Resolution ScanSAR Mode (CRS), and High-Resolution Spotlight Mode (HRS). These modes allow the satellite to capture data with different levels of detail and coverage. The resolution capability of the EOS-04 satellite ranges from 1 m to 50 m, enabling data acquisition at various spatial resolutions.

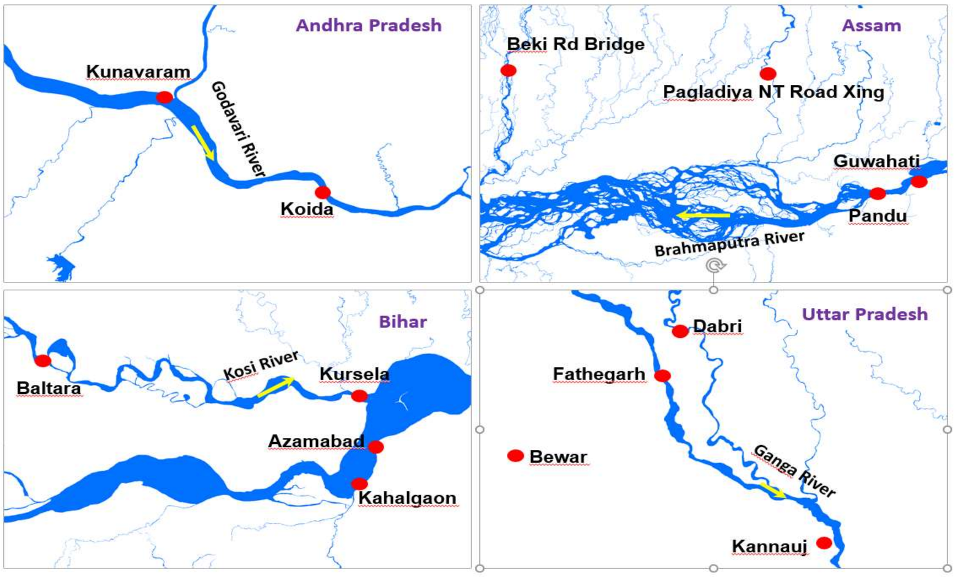

Note:*Blue colour represents permanent water bodies in each study area*

Figure.2. River gauge station locations at Andhra Pradesh, Assam, Bihar and Uttar Pradesh.

Formatted: Line spacing: single

Formatted: Font: Not Bold

3.2. Field Measurements:

Typically, water levels are measured using gauge stations installed along rivers. The Central Water Commission (CWC) of India provides hourly field measurements from these gauge stations, as illustrated in Figure 2, for various sites, and makes the information available on their website (https://ffs.india-water.gov.in/). Water levels recorded at the times corresponding to satellite acquisitions across all study areas are compared with the interpolated levels derived from the Trend Surface Analysis

(TSA). Table 3 presents the field-measured water levels from gauge stations corresponding to the specific dates and times of satellite acquisitions.

Table.4 Field-Measured Water levels from Gauge stations in the study area

S.No	**Study Area**	**Water Gauge Station Name**	**Field Measured Water Levels(meters)**
1	Andhra Pradesh	Kunavaram	41.02
2		Koida	39.72
3	Assam	Beki Rd Bridge	44.92
4		Pangladiya NT Road Xing	52.84
5		Pandu	47.25
6		Guwahathi	48.19
7	Bihar	Baltara	34.9
8		Kahalgaon	31.08
9		Azamabad	30.54
10		Kursela	29.98
11	Uttar Pradesh	Dabri	137.18
12		Fathegarh	137.78
13		Kannauj	125.67
14		Bewar	138.32

4. Methodology

The process of quickly estimating flood depth using the Digital Elevation Model and EOS-04 satellite involves several steps. These include generating a radar backscatter coefficient image from the raw satellite image, extracting the flood inundation layer using an automated tile-based segmentation method, obtaining terrain information prior to the flood event using digital elevation model, interpolating floodwater surface levels through Trend Surface Analysis, and determining the spatial flood depth. The methodology is illustrated in the flow chart as shown in Figure 3~~.~~(a) and Figure3(b). A customized Python code has been developed specifically for automated flood mapping and depth estimation using ArcGIS and GDAL libraries.

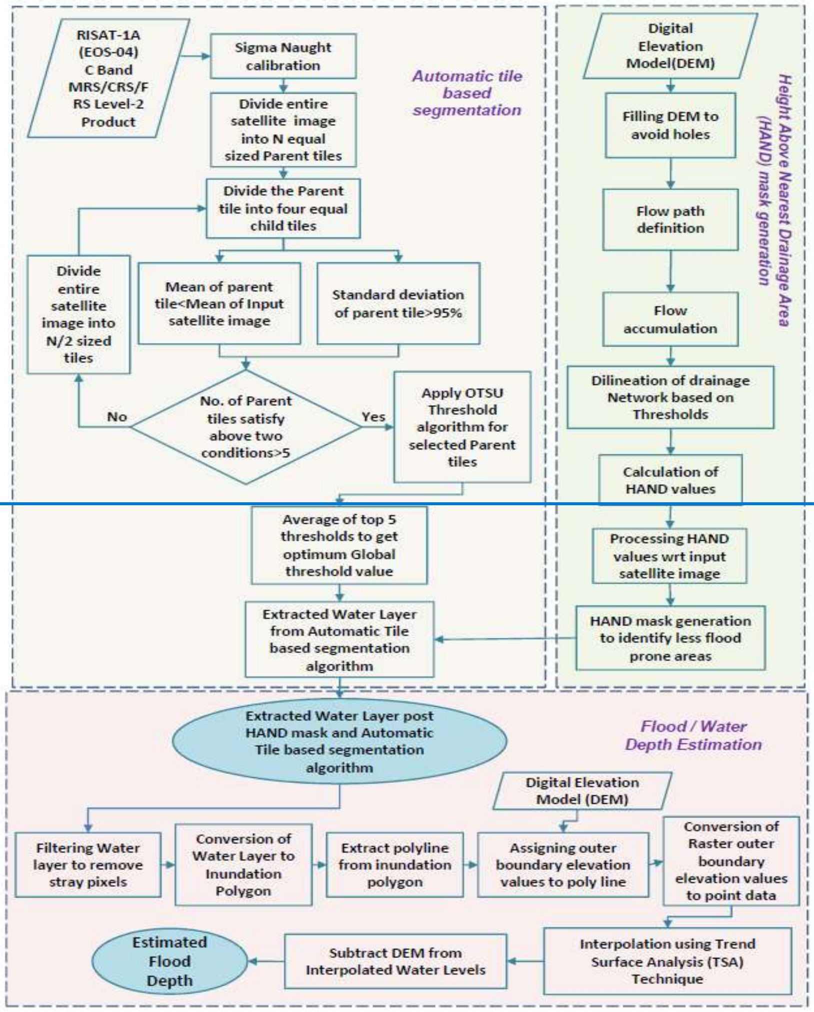
RISAT-1A (EOS-04) C Band MRS/CRS/FRS Level-2 Product
Sigma Naught calibration
Automatic tile based segmentation
Divide entire satellite image into N equal sized Parent tiles
Divide the Parent tile into four equal child tiles
Divide entire satellite image into N/2 sized tiles
Mean of parent tile<Mean of Input satellite image
Standard deviation of parent tile>95%
No
No. of Parent tiles satisfy above two conditions>5
Yes
Apply OTSU Threshold algorithm for selected Parent tiles
Average of top 5 thresholds to get optimum Global threshold value
Extracted Water Layer from Automatic Tile based segmentation algorithm
Digital Elevation Model(DEM)
Filling DEM to avoid holes
Flow path definition
Flow accumulation
Dilineation of drainage Network based on Thresholds
Calculation of HAND values
Processing HAND values wrt input satellite image
HAND mask generation to identify less flood prone areas
Height Above Nearest Drainage Area (HAND) mask generation
Extracted Water Layer post HAND mask and Automatic Tile based segmentation algorithm
Flood / Water Depth Estimation
Digital Elevation Model (DEM)
Filtering Water layer to remove stray pixels
Conversion of Water Layer to Inundation Polygon
Extract polyline from inundation polygon
Assigning outer boundary elevation values to poly line
Conversion of Raster outer boundary elevation values to point data
Interpolation using Trend Surface Analysis (TSA) Technique
Subtract DEM from Interpolated Water Levels
Estimated Flood Depth

185

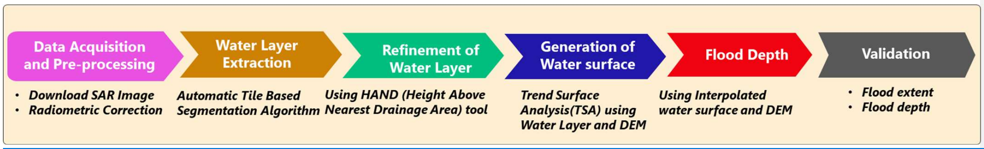

Figure.3. (a). Steps of methodology

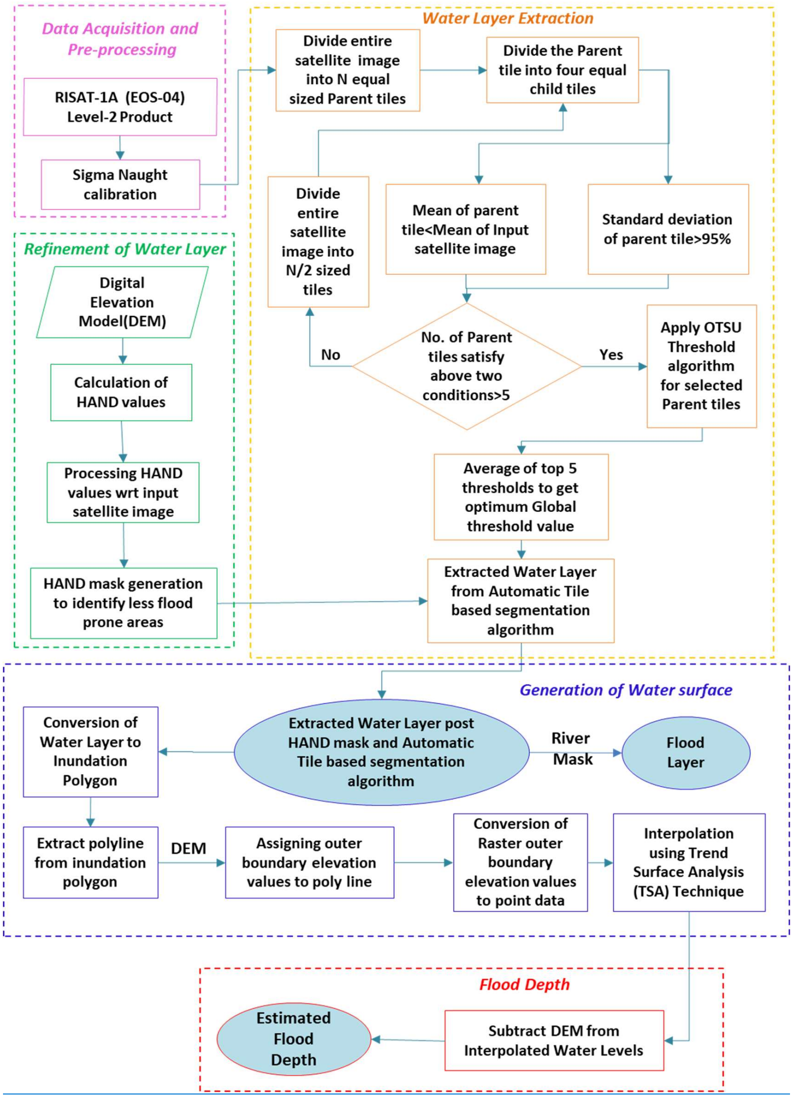
Data Acquisition and Pre-processing
RISAT-1A (EOS-04) Level-2 Product
Sigma Naught calibration
Water Layer Extraction
Divide entire satellite image into N equal sized Parent tiles
Divide the Parent tile into four equal child tiles
Divide entire satellite image into N/2 sized tiles
Mean of parent tile<Mean of Input satellite image
Standard deviation of parent tile>95%
No
No. of Parent tiles satisfy above two conditions>5
Yes
Apply OTSU Threshold algorithm for selected Parent tiles
Average of top 5 thresholds to get optimum Global threshold value
Extracted Water Layer from Automatic Tile based segmentation algorithm
Refinement of Water Layer
Digital Elevation Model(DEM)
Calculation of HAND values
Processing HAND values wrt input satellite image
HAND mask generation to identify less flood prone areas
Generation of Water surface
Conversion of Water Layer to Inundation Polygon
Extracted Water Layer post HAND mask and Automatic Tile based segmentation algorithm
River Mask
Flood Layer
Extract polyline from inundation polygon
DEM
Assigning outer boundary elevation values to poly line
Conversion of Raster outer boundary elevation values to point data
Interpolation using Trend Surface Analysis (TSA) Technique
Flood Depth
Estimated Flood Depth
Subtract DEM from Interpolated Water Levels

Figure.3(b). Detailed Flow chart for Methodology

~~4.1 Generation of radar back scatter coefficient image~~

~~Indian Space Research Organisation (ISRO) 's Bhoonidhi portal is a web interface that hosts~~4.1 Data Acquisition and Pre-processing

Any multi-sensor satellite data~~. Images~~ which is acquired ~~from~~past the ~~EOS-04~~flood event by satellite ~~are directly~~is hosted in Indian Space Research Organisation (ISRO)'s Bhoonidhi portal and can be downloaded~~ from the Bhoonidhi portal. It is necessary to apply~~. Pre-processing of EOS-04 data involves both geometric and radiometric corrections before application of data for flood extraction (A. V. Suresh Babu et al., 2024). Geometric correction ~~to Level 2 product SAR images to truly enable~~ensures the spatial accuracy of the ~~original Digital Numbers (DN) pixel values to represent the radar backscatter of the reflecting surface. Radiometric correction is essential if one has to compare SAR images acquired~~SAR data by aligning it with ~~different sensors~~ a coordinate system or ~~acquired from the same~~correcting distortions caused by sensor ~~at different~~geometry, Earth's curvature, and terrain variations. While radiometric correction involves adjusting the pixel values in the SAR data to accurately reflect the actual backscattered signal (Converts raw digital numbers (DNs) into physical quantities such as backscatter intensity) compensating for system and environmental effects. This ensures consistency across sensors and acquisition times~~, in different modes.~~. Radar backscatter represents the intensity of the radar signal reflected back to the sensor from the Earth's surface, providing valuable insights into surface roughness, moisture content, and material properties. By analysing radar backscatter, water bodies can be accurately identified, surface conditions can be properly assed, land and water classification can be improved in remote sensing applications. Radar backscatter coefficient values, i.e., Sigma Nought (σ_o), ~~are~~for EOS-04 satellite image is computed as per the following equation~~:~~ (1):

$$\sigma_o(dB) = 20 * \log_{10}(DN) + 10 * \log_{10} \sin \theta_{inc} - CF$$

~~where~~(1) Where DN represents digital number (amplitude in Level-2 products), $\theta_{inc}$is the per pixel local incidence angle and CF is the Calibration Factor.

4.2 ~~Methodology for~~Water Layer Extraction~~ of Flood Layer~~

The ~~extraction process for the Flood Layer~~water layer from the ~~Sigma naught~~radiometrically calibrated image ~~involves four main steps. These include~~is extracted using ~~an Automatic tile-based segmentation method, obtaining a global threshold value, calculating HAND (Height above the Nearest Drainage Area) mask and extracting the Flood layer.~~

~~4.2.1~~ the Automatic Tile-Based ~~Classification~~Segmentation Method~~ for extraction of Water layer~~

~~The Automatic tile-based segmentation method analyses the image in sections called image tiles. This approach divides the entire SAR image into non-overlapping tiles of equal n x n pixels, known as parent tiles. If an equal size~~, which involves partitioning ~~of~~ the image ~~is not feasible, adjustments can be made to the last column and row~~ into tiles~~ to ensure that the~~

~~remaining~~, specific criteria-based tile selection, calculating thresholds, and classifying the image into water and non-water areas (Martinis et al., 2015) as illustrated in Figure 4. The image is partitioned into non-overlapping tiles ~~have~~of equal size (n x n ~~pixel size. These n-sized~~pixels), referred to as parent tiles. If perfect partitioning is not possible, the last row and column tiles are ~~further~~adjusted to ensure they remain n x n pixels. Each parent tile is then subdivided into ~~4~~four equal-sized child tiles. For threshold calculation, ~~certain~~ tiles are selected based on two conditions: ~~(i) the~~

1. The mean ~~individual~~ radar backscatter value of the parent tile should be ~~less~~lower than the mean ~~radar~~ backscatter value of the entire ~~SAR~~ image ~~to ensure that~~, ensuring the ~~selected~~ tiles are ~~within the SAR image and are~~ located ~~on~~near the boundary between water and non-water areas~~; and (ii) the~~.
2. The standard deviation of the parent tile ~~is greater than~~must exceed 95~~%,~~% of the image's overall standard deviation, indicating significant variation within the ~~data and leading to a better~~ tile, which enhances the classification of water and non-water areas. ~~This process is illustrated in Figure 4.~~

Formatted: List Paragraph, Numbered + Level: 1 + Numbering Style: 1, 2, 3, … + Start at: 1 + Alignment: Left + Aligned at: 0.63 cm + Indent at: 1.27 cm

~~Andrew Twele et al., (2016) analysis shows that if fewer than five percent of~~If parent tiles that meet the specified conditions is less than 5% of total tiles, the ~~SAR~~ image is ~~divided~~subdivided into smaller tiles (n/2 × n/2 ~~x n/2-sized parent tiles. The~~) and the standard deviation ~~condition for selecting parent tiles can be lowered~~threshold is then relaxed to 90%, and the process is repeated until the ~~desired condition is met. All the~~selected tile is sufficient. Once the necessary tiles are chosen, all parent tiles that satisfy ~~the above two~~both conditions are ~~subjected to~~processed using the ~~OTSU threshold~~Otsu thresholding technique. The ~~mean~~global threshold value is calculated as the average of the individual thresholds from the selected tiles and is used to ~~calculate the global threshold value for classifying the SAR image. This threshold value helps to distinguish between~~ classify the SAR image into water and non-water areas. This methodology is summarized in the flowchart presented in Figure 3(b).

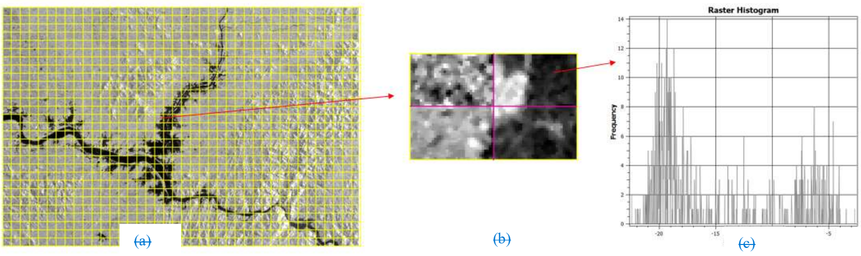

~~(a)~~ ~~(b)~~ ~~(c)~~

(a) (b) (c)

Figure.4. Automatic Tile based segmentation of SAR image (a)Division of SAR image into n parent tiles (b)Division of parent tile to 4 child tiles (c)Histogram of one child tile

4.~~2.2. Delineation~~3. Refinement of ~~Flood layer~~Water Layer

~~It is crucial to ensure that false water areas, such as shadows in steep terrain, are excluded from flood detection. In this context, the filtering process aims to enhance~~To improve the accuracy of water ~~detection using the~~ classification and eliminate false water areas such as shadows and stray pixels caused by speckle noise, the Height Above Nearest Drainage (HAND) tool is employed. HAND is a terrain model that standardizes topography relative to the drainage network and ~~is used to characterize~~characterizes local drainage ~~potentials~~potential. In a HAND raster, each pixel ~~value~~ represents the vertical distance (in meters) from that point to the nearest drainage channel.

~~The~~ HAND ~~model leverages DEM inputs to rapidly assess~~ tool facilitates the rapid identification of non-flooded areas~~. Creating a HAND raster image from a DEM involves several steps, as illustrated in Figure 3. These steps include generating a seamless, hydrologically corrected DEM by filling holes, defining flow paths with Flow Direction, identifying the drainage network using Flow Accumulation, and calculating the Height Above Nearest Drainage (HAND) using the D8 flow distance function. The HAND raster provides spatially distributed values that represent the elevation difference between a given point (pixel) and the nearest stream,~~ by restricting the flood areas up to HAND Value of 15 m following the local drainage direction toward the channel where ~~the flow enters~~ water flows. According to Nobre et al. (2015), regions with HAND values greater than 15 ~~exhibit reduced vulnerability~~meters are less vulnerable to flooding. ~~Consequently, an exclusion mask based on these HAND values is generated for this study. After~~ Hence applying the HAND mask~~, a suitable water layer is derived using data from the EOS-04 satellite. This~~ refines the water layer ~~undergoes further processing to create a~~ , significantly reducing misclassification and subsequently producing the flood ~~map, which overlays the derived water layer with a mask delineating~~ layer by subtracting a permanent ~~water bodies, such as~~ rivers ~~and lakes.~~mask. The creation of a HAND raster from a DEM involves several steps, illustrated in Figure 3(b). These steps include:

- ~~4.3. Methodology for Flood depth Estimation~~Generating a seamless, hydrologically corrected DEM using ~~Trend~~the Fill tool.
- Defining flow paths using the Flow Direction function.
- Identifying the drainage network through Flow Accumulation.
- Calculating the HAND values using the D8 flow distance algorithm

4.4. Generation of Water Surface ~~Analysis (TSA) Technique~~

~~The~~To estimate flood depth ~~in this methodology~~, it is ~~estimated by~~necessary to generate a water surface using ~~the~~only a 2D inundated water layer and ~~DEM as inputs. First, a water layer is generated polygon using the Automatic Tile-based segmentation method and then converted to polygon. Then, a polyline is created from the polygon to form the outer boundary segments. This polyline is then converted to a raster. Subsequently, the corresponding outer boundary elevation values from the DEM are assigned to this raster. An interpolation technique is then utilized to estimate water surface elevation values for~~

~~all the pixels inside the flood boundary. In this paper, we employed the~~a Digital Elevation Model (DEM) as input data using Trend Surface Analysis (TSA). TSA generated water surface offers a notable advantage over traditional hydrodynamic models, which are often data-intensive. This streamlined approach provides a simplified yet effective solution for flood depth estimation. Trend Surface Analysis ~~(TSA) technique for interpolating the elevation values for the entire inundated surface. TSA belongs to the Global Fit interpolation technique, which calculates a single function describing a surface covering the entire map area, as opposed to the Local Fit method which estimates the surface at interpolation points by selecting the nearest data/reference points.~~

~~Trend surface analysis is a powerful method that~~ uses global polynomial interpolation to ~~create~~generate a smooth surface defined by a mathematical function ~~based on~~derived from input sample points. This ~~method~~technique effectively captures gradual changes and coarse-scale patterns ~~within~~in the data, producing a smooth surface ~~representing~~that reflects the ~~gradual~~overall trend across the area of interest (Morton et al., 1974). ~~. Trend surface analysis involves~~TSA achieves this by fitting a polynomial function to known data points (outer boundary elevations points) and using this function to ~~make predictions for~~predict values at locations where data is ~~not available. The accuracy of the interpolated surface is indicated by the root mean square (RMS) error, with a lower error value signifying a closer representation of the input points. Mathematically, this technique is represented as below: Observed elevation value at a point on the surface = Predicted Elevation value using TSA method at that point+ residual at that point which is illustrated in following equation~~ ~~$Z_{observed}$~~ =unavailable inside the flood extent. In this study, the outer boundary elevation values derived from the DEM for the inundated water layer are used as input for the interpolation process. ~~$f(x_i, y_i) + r_i$(2)~~

~~$Z_{observed}$= The observed elevation value at the i^{th} point~~

~~x_i= The coordinate on the X-axis ie Latitude at the i^{th} point~~

~~y_i=The coordinate on the Y-axis ie Longitude at the i^{th} point~~

~~r_i=residual at the i^{th} point~~

~~$f(x_i, y_i)$denote a polynomial function.~~

Based on the findings of Cohen et al. (~~2007~~2017), Huang et al. (2014), Brown et al. (2016), and Cian et al. (2018), it is assumed that the water surface in flooded areas is flat when calculating flood depth, this paper implemented the first-degree polynomial equation in TSA

Mathematically, the observed elevation at any point along the outer boundary of inundated water surface can be expressed as the sum of the predicted elevation from TSA and the residual error at that point:

$$Z_{observed} = f(x_i, y_i) + r_i$$

$Z_{observed}$= The observed elevation value at the i^{th} point inside water surface

$f(x_i, y_i)$~~. Since the elevation variations in all four case studies are gradual, this paper utilizes the linear trend interpolation technique for estimating flood depth. The linear trend surface interpolator uses polynomial regression to create a least-squares surface from the input points. This approach allows for customization and flexibility in the analysis process by providing control over the polynomial order used to fit the surface.i.e.~~

= Polynomial function that predicts the elevation based on the coordinates x_i (latitude) and y_i(longitude).

r_i=represents the residual at the i^{th}point, which is the difference between the observed and predicted elevation.

The first-degree polynomial equation used in this study is defined as:

$$f(x_i, y_i) = ax_i + by_i + c$$

where a, b and c are constants that define the coefficients of the polynomial.

~~The aim of Trend Surface Analysis (TSA) is to determine the most suitable surface based on outer boundary elevation values, thereby uncovering the fundamental patterns of gradients and contours within the sample space (Morton et al., 1974).~~ In real-world topographic surfaces, ~~it is unlikely that any~~ observed ~~surface will exactly follow an idealized trend. The observed elevation values will either lie above or below the trend surface, resulting in residuals or prediction errors at each point.~~ elevations rarely align perfectly with the predicted trend. Residuals r_i quantify the discrepancy:

- A positive residual ~~(above zero)~~ indicates that the observed elevation is above the trend surface ~~lies below the observed surface at that location, while a~~.
- A negative residual indicates that the observed ~~surface lies~~elevation is below the ~~predicted~~ trend surface. ~~Each combination of~~

To determine the optimal coefficients a,~~,~~ b~~,~~, and c ~~would generate a different inclined plane. Some of these surfaces would be good if the observed points were close to them, resulting in low residual values, whereas other surfaces would be poor if the observed values were distant from them. It would be useful to find a method of determining the very best possible combination of a, b, and c. To choose those constants~~, the least squares criterion is ~~used, which finds the combination of a, b, and c that minimizes~~employed, minimizing the sum of ~~squares of~~squared residuals (S~~).~~):

$$S = \sum_{i=1}^{N} (r_i^2)$$

~~Where~~Where S represents the sum of squared residuals and r_i ~~$= Z_{observed} - (ax_i + by_i + c)$~~ ~~To estimate flood depth in this paper, the Trend Surface Analysis technique (TSA)~~ is ~~applied to~~ the residual at the i^{th} point

~~Water Layer~~The process for deriving the TSA-interpolated surface is illustrated in Figure 5. First, the 2D water layer, obtained from the Automatic ~~flood mapping output. The water layer is~~Tile based Segmentation method and the HAND tool, as shown in Figure 5(a), needs to be converted into ~~a~~ polygon~~,~~ form. This layer is then transformed into a ~~polyline and a~~polygon that retains only the outer boundary segments. Next, the polygon is converted into raster~~. Using~~ format, and the ~~respective DEM,~~corresponding outer boundary elevation values ~~for the water layer~~ are ~~extracted and~~ assigned ~~to the raster. As~~from the Digital Elevation Model (DEM). Since the TSA technique ~~works only~~ operates exclusively on point data, ~~this~~the raster is then converted to ~~point form. Subsequently, the surface is interpolated using the TSA technique based on the flood outer boundary~~ point ~~data.~~form, as depicted in Figure 5(b). A first-degree polynomial surface is fit to the outer boundary elevation values.

Predicted elevations are computed across the inundated area, producing an interpolated TSA water surface as illustrated in Figure 5(c). The resulting TSA ~~Interpolated~~interpolated surface provides estimated water surface levels in meters~~. Finally, the~~

Formatted: Justified

Formatted: Font: Times New Roman, Not Italic

Formatted: Justified

~~estimated Flood depth is determined by subtracting the Digital Elevation Model (DEM) from the interpolated water levels. This methodology is further explained in the figure 5.~~

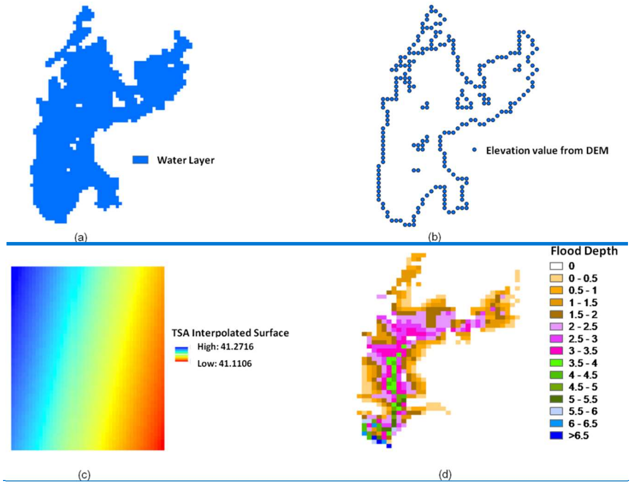

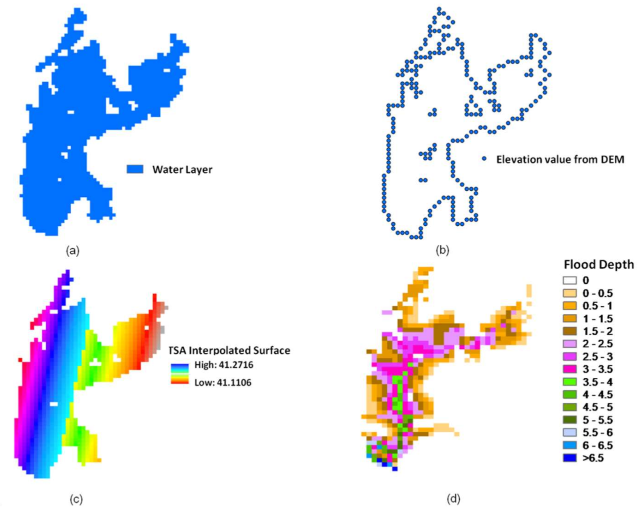

~~**Figure 5**~~

Figure5: Methodology for flood depth estimation using TSA technique: (a) Water layer created using the Automatic Tile-based segmentation technique~~.~~ and HAND tool. (b) Elevation values extracted for the outer boundary water layer from the Digital Elevation Model (DEM) as points. (c)Interpolated surface is generated using these elevation points through Trend Surface Analysis (TSA)~~.(~~). (d)Flood depth is estimated by subtracting DEM values from the interpolated water levels (above mean sea level).

4.~~ ~~5. Flood Depth

The calculation of flood depth is achieved by subtracting the Digital Elevation Model (DEM) from the water levels interpolated by the TSA. The resulting depth is expressed in meters, as depicted in Figure 5(d).

5.Results and Discussion

This research ~~estimates~~ focuses on automated rapid flood inundation ~~areas from SAR image, derives flood boundaries,~~ and ~~simulates~~ depth estimation using Synthetic Aperture Radar (SAR) imagery (EOS-04 data) integrating Automatic Tile-Based Segmentation Method and the Height above Nearest Drainage (HAND) tool is validated for flood ~~contours and surfaces based on~~ extent against cloud-free optical satellite data for Bihar and Uttar Pradesh, as detailed in Section 5.1. Flood water depth is estimated on all study areas and validated as per in section 5.2. Accurate digital elevation models~~. The spatial resolution and accuracy of the digital elevation models~~ (DEMs) are ~~crucial~~critical for ~~extracting~~determining floodwater depth~~. In this study,~~, but high accurate DEMs are not available all places hence it is required to assess the sensitivity of flood depth against DEM characteristics. This study uses a high-resolution 5m LIDAR DEM ~~is used~~and the Copernicus 30m FABDEM for~~ one case study,~~ the Godavari River ~~reach, while simultaneously using Copernicus FAB 30m DEM~~ to assess ~~the~~flood depth sensitivity ~~of the DEM~~, as described in ~~determining flood depth. The results from three other study areas~~Section 5.2.1. Flood depth estimation using Trend Surface Analysis (TSA) is conducted for the Godavari, Ganga, Brahmaputra, and Kosi rivers~~ are also presented. Additionally, the~~. The accuracy of ~~the~~TSA-derived flood depth ~~values derived from Trend Surface Analysis (TSA)~~estimates is ~~evaluated~~assessed by comparing them with field~~ based~~ -measured river water levels ~~provided by CWC on that particular day and time. It is also being compared~~recorded by the Central Water Commission (CWC) for corresponding dates and times. Additionally, further comparisons with ~~FWDET~~the Flood Water Depth Estimation Tool (FWDET) are comprehensively detailed in Section 5.2.2.

45.1. Flood Inundation Area Estimation and validation

The flood inundation layer is ~~delineated using the Automatic Tile Based Classification Method on SAR data, with the HAND (Height Above Nearest Drainage) tool applied to eliminate false water areas and accurately identify actual flood water. During the flood disaster, it is challenging to conduct~~created using proposed method fromEOS-04 data. Conducting fieldwork for flood map validation~~. Hence~~ during a flood disaster is often challenging. Therefore, the accuracy of ~~this~~the delineated flood layer is ~~evaluated~~assessed using a cloud-free optical satellite ~~cloud freeLandsat-8~~ image from Landsat-8 of

Formatted: Left

15m resolution, which was acquired on the same date i.e., ~~15th August 2023 similar to~~August 15, 2023as the EOS-04 ~~date~~data of 18 m in the Uttar Pradesh study area. ~~The delineation of~~ Additionally, a Resourcesat-2 LISS-4 image of 5.8m, also obtained on the same date as EOS-04 i.e., September 3, 2023 was used for the Bihar study area. To extract water ~~spread in Landsat-8 image is carried out using~~ extent from the optical images, standard unsupervised classification techniques were applied using ERDAS ~~imaging~~Imagine software. The results of this analysis are ~~shown~~presented in ~~figure~~Fig. 6.

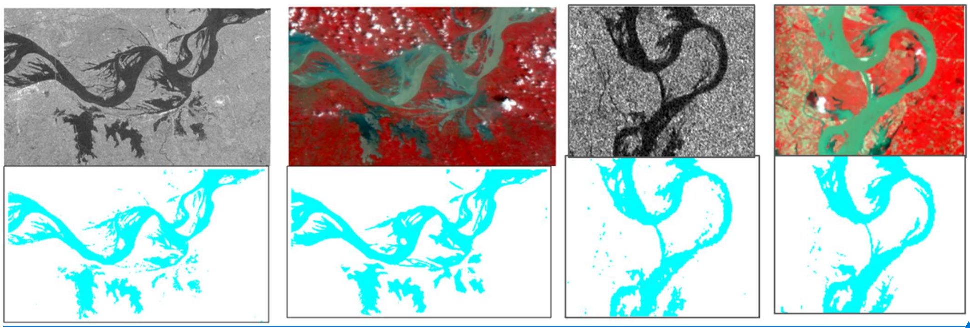

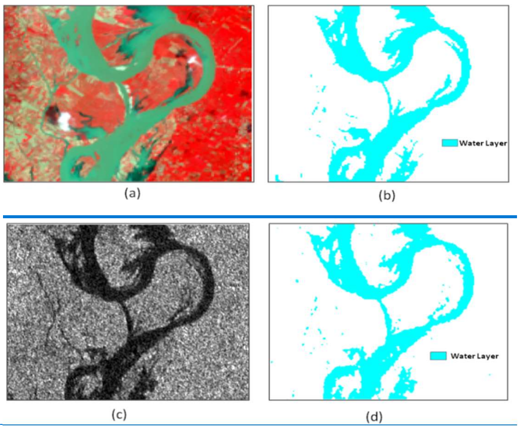

(a) (b)

(c) (d)

Figure 6: Optical satellite data and EOS-04 data comparison ~~(a) shows the optical Landsat-8 data of Resolution 15m in Uttar Pradesh~~. (a) EOS-04 data and the delineated flood layer using Automatic Tile-Based Segmentation Method and HAND tool in Bihar study area. ~~(b)Water~~ (b) Resourcesat-2 LISS-4 data and the flood inundation layer extracted ~~from optical data~~ using

Formatted: Font: Bold

Formatted: List Paragraph, Numbered + Level: 1 + Numbering Style: a, b, c, … + Start at: 1 + Alignment: Left + Aligned at: 1.93 cm + Indent at: 2.57 cm unsupervised classification~~. (c) EOS-04 data~~ in ~~the same~~Bihar study area~~ of Landsat-8 data. (d) Water ~~. (c) EOS-04 data and the delineated flood layer using Automatic Tile-Based Segmentation Method and HAND tool in Uttar Pradesh study area. (d) LANDSAT-8 data and the flood inundation layer extracted ~~from EOS-04 data using Automatic Tile based segmentation algorithm~~ using unsupervised classification in Uttar Pradesh study area

As a part of accuracy test for flood extent using proposed method, Confusion matrix and performance metrics is computed for Bihar and Uttar Pradesh study area with respect to respective optical datasets as detailed in

table 5 and table 6.

Table 5: Confusion Matrix for Flooded and Non-Flooded Areas in Bihar and Uttar Pradesh study areas

~~As a part of accuracy test, statistical area covered under water delineated from Landsat-8 and EOS-04 image is computed and tabulated in table 3. It is observed that the~~ **Uttar Pradesh**		
Actual/Predicted	**Flooded**	**Non-Flooded**
Flooded	174,506	6,391
Non-Flooded	11,577	37,686

~~Area computed~~**Bihar**	~~Optical data~~	~~SAR data~~
Actual/Predicted	~~446 Ha~~**Flooded**	~~455 Ha~~**Non-Flooded**
Flooded	8,534,283	116,598
Non-Flooded	513,381	2,038,290

~~**Table:3:** Statistical area covered under water~~

Table 6: Performance metrics for Flooded Areas in Bihar and Uttar Pradesh study areas

Study Area	**Precision**	**Recall**	**F1-Score**	**Accuracy**
Bihar	95%	80%	87%	**94%**
Uttar Pradesh	86%	76%	81%	**92%**

Split Cells
Deleted Cells
Formatted: Line spacing: 1.5 lines
Formatted: Strong
Deleted Cells
Formatted Table
Formatted: Font: Bold
Formatted: Font: Bold
Formatted: Font: Bold
Formatted: Line spacing: 1.5 lines

The flood delineation accuracy ~~using Automatic tile-based classification method on SAR data is approximately 94~~for the Bihar and Uttar Pradesh study areas exceeds 90% when compared to optical data~~. It is also understood from~~ as per table 6. However, certain discrepancies are observed as per table 5 due to the ~~above figures, that the variation of mismatch is because, in the shallow water areas of flowing waters,~~ characteristics of microwave data~~ showing as no water which is not true from~~. In shallow flowing water areas, microwave sensors may incorrectly classify these regions as dry, unlike optical data~~. ~~, which accurately identifies the presence of water. Additionally, microwave data sometimes misinterprets moisture-laden areas as flooded, leading to overestimations.

~~From~~Despite these ~~results, it is observed that~~limitations, the Automatic Tile~~-~~-Based Segmentation Method ~~is deemed appropriate for deriving~~combined with the HAND tool proves effective for generating flood maps ~~in rapid mode~~rapidly using ~~SAR~~EOS-04 data. ~~As Flood~~Since flood depth ~~result depends~~estimation relies on the delineated flood extent from SAR ~~image~~images, this method ~~is useful for automatic detection of water layer in the SAR image~~offers a reliable approach for automatically detecting water layers, enabling efficient and accurate flood mapping in critical situations.

~~4~~5.2. Floodwater Depth Estimation and validation

~~The shape of flood layers varies across different areas, with some regions appearing wide, indicating a gentle slope, and others being narrow along rivers, suggesting a steeper gradient, as observed in the aforementioned case studies. There is an increasing demand for accurately determining flowing water surfaces to precisely estimate flood depths. Typically, the flowing water surface is derived through two steps: firstly, by collecting elevations along the flood inundation boundary, which represent varying heights of discrete points, and secondly, by fitting a surface across these elevation points using commonly used interpolation methods.~~

~~4~~5.2.1. ~~Comparison~~Sensitivity of ~~DEMs in flood water depth estimation~~Flood Depth with DEM characteristics

The accuracy of floodwater depth measurements depends significantly on the accuracy and spatial resolution of the Digital Elevation Model (DEM) as it plays a major role in interpolation of flood water depth. To assess this, an analysis was conducted in the Godavari flood plain area, utilizing two different DEM datasets. One DEM was derived from LiDAR data with a 5-meter spatial resolution and vertical accuracy of 15 cm, while the other was obtained from the public domain, specifically the Copernicus FABDEM, with an 8-meter vertical accuracy and 30-meter spatial resolution. This comparative study aims to evaluate the impact of public domain DEMs on the accuracy of flood water depth estimation. Here, the flood depth is estimated in Godavari Flood plain study area using Trend Surface Analysis (TSA) Technique. The results of this analysis are presented in the figure 7 below. A scatter plot is drawn for comparison of flood depth values estimated using TSA technique for LIDAR and Copernicus DEMs.

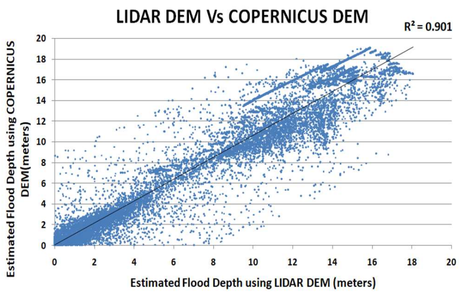

Figure 7: Plot between LIDAR DEM and Copernicus DEM derived Flood depths

The scatter plot above ~~shows~~indicates that 90% of ~~the~~ flood depth points derived from LiDAR and Copernicus DEMs match closely~~ match. Discrepancies~~. The areas where discrepancies occur are predominantly ~~occur~~ in ~~areas with~~ steep ~~slopes where~~slope regions having elevation changes rapidly. Therefore, accurate LiDAR-derived DEMs are essential for estimating flood depths in steep areas. In contrast, for ~~areas with~~ gentle ~~slopes, the Copernicus~~slope areas, COPERNICUS DEM~~,~~ with ~~its~~a 30-meter spacing ~~provides~~and vertical accuracy of 8 meters provide sufficiently accurate flood depth estimates~~,~~ as depths are relative ~~to~~ heights.

5.2.2 Results of Flood Depth Estimation and validation

The shape of flood layers varies across different areas, with some regions appearing wide, indicating a gentle slope, and others being narrow along rivers, suggesting a steeper gradient, as observed in the aforementioned case studies. There is an increasing demand for accurately determining flowing water surfaces to precisely estimate flood depths. Typically, the flowing water surface is derived through two steps: firstly, by collecting elevations along the flood inundation boundary, which represent varying heights of discrete points, and secondly, by fitting a surface across these elevation points using ~~4~~proposed interpolation methods.

5.2.2.1 Derivation of Flood depths using TSA technique in Study Areas

Given the dynamic nature of ~~river elevations and~~ varying water levels of flowing river at different locations, employing trend surface analysis becomes essential for simulating the ~~flood~~exact water surface, especially in large flooded areas with gentle slopes. This process involves calculating floodwater depths based on DEM Resolution at specific locations, such as pixels. For Andhra Pradesh study area, LIDAR DEM derived flood water depth using TSA is illustrated in fig 8. For the remaining three study areas such as Bihar, Assam and Uttar Pradesh, publicly available Copernicus DEMs is used to estimate flood water depth using TSA technique. The ~~figure 8~~figure8 below ~~illustrates~~illustrate the flood depths in four areas of gentle slope. Figure 8(e) represents the legend followed in the flood water depth estimation ~~(in meters)~~ in all the four study areas.

From Figures 8(a), 8(b), 8(c), and 8(d), it is evident that the flood depth is greater in river areas and it is represented in blue colour. Flood depths derived from TSA technique are smooth and continuous.

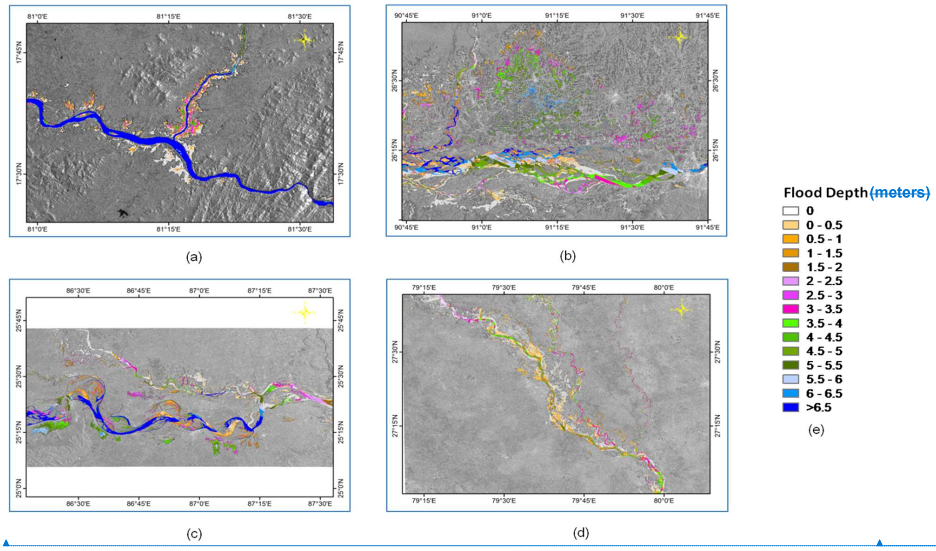

Figure:8: Flood depths calibrated using ~~STA~~TSA Technique for (a)Andhra Pradesh (b)Assam (c)Bihar and (d) Uttar Pradesh States (e)Legend for the Flood depth in meters

~~4~~5.2.~~3~~2.2 Validation of Flood depth results

The water levels ~~that have been~~ derived using the Trend Surface Analysis (TSA) technique in four case study areas ~~is~~are compared ~~against~~with field-based water level measurements ~~at~~from gauge ~~station~~stations provided by the Central Water Commission (CWC ~~on~~) for the same ~~particular day~~date and time. ~~The below figure~~Figure 9 ~~describes~~illustrates the method ~~of comparison between~~ used to compare the TSA-derived water levels and the field~~-based measurement and TSA output.~~ measurements.

At each CWC ~~provided River~~river gauge station, TSA~~-~~-interpolated water levels ~~are~~were computed. ~~At that particular~~The field-measured water levels at the corresponding location, date, and time~~, field measured Water level is taken~~ served as reference points for the comparison study. ~~The below table 4 shows the~~Table 7 presents the comparison results and also includes a comparison ~~study. TSA interpolated~~against water levels ~~are also compared against~~estimated using the Flood Water Depth Estimation (FWDET) method. ~~Water level is calculated using~~ The FWDET ~~method~~water level estimations were

Formatted: English (United States)
Formatted: Font: 8 pt
Formatted: English (India)
Formatted: English (India)
Formatted: English (India)
Formatted: English (India)
Formatted: English (India)
Formatted: English (India)
Formatted: English (India)
Formatted: English (India)
Formatted: English (India)
Formatted: English (India)
Formatted: Font color: Text 1, English (India)
Formatted: Font color: Text 1, English (India)
Formatted: English (India)
Formatted: English (India)
Formatted: English (India)
Formatted: English (India)
Formatted: English (India)
Formatted: English (India)
Formatted: English (India)
Formatted: English (India)
Formatted: English (India)
Formatted: English (India)
Formatted: English (India)
Formatted: English (India)
Formatted: English (India)
Formatted: English (India)

performed in ~~Open Source~~the open-source QGIS environment ~~by taking~~, using the same study ~~area's inundated~~area's inundation water layer and a Digital Elevation Model (DEM) as ~~input.~~inputs

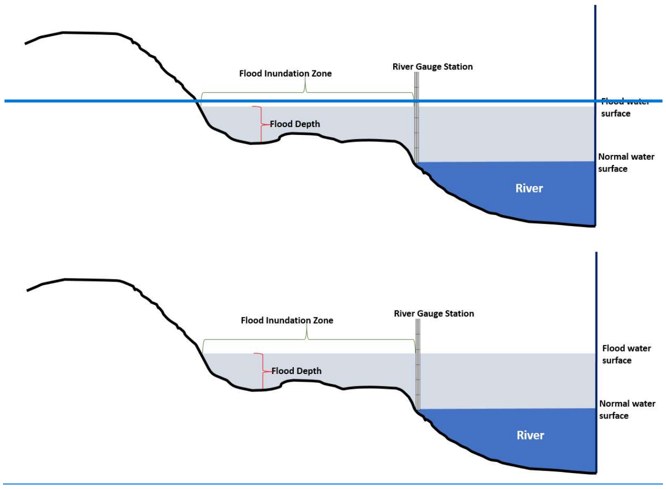

Figure 9: Pictorial representation of Flood plain and River Gauge station

S.No	Water Gauge Station Name	Field Measured Water Levels	TSA Interpolated Water Levels in meters	FWDET Interpolated Water Levels in meters
ANDHRA PRADESH				
1.	Kunavaram	41.02	40.63	46.62
2.	Koida	39.72	39.68	42.19
ASSAM				
1.	Beki Rd Bridge	44.92	46.4	41
2.	Pangladiya NT Road Xing	52.84	51.5	50.5
3.	Pandu	47.25	47.12	41.5
4.	Guwahathi	48.19	48.6	42
BIHAR				

Formatted: English (India)
Formatted: English (India)
Formatted: English (India)
Formatted: English (India)
Formatted: English (India)
Formatted: English (India)
Formatted: English (India)
Formatted Table

1.	Baltara	34.9	34.08	32.85
2.	Kahalgaon	31.08	31.459	24
3.	Azamabad	30.54	30.16	24
4.	Kursela	29.98	28.98	27
UTTAR PRADESH				
1.	Dabri	137.18	138.6	136.21
2.	Fathegarh	137.78	137.4	136.05
3.	Kannauj	125.67	126	125.82
4.	Bewar	138.32	139.04	150.3

Table ~~4~~7: Comparison study of Water levels among between field measurements, TSA and FWDET

Formatted: Font: Times New Roman, 10 pt, Font color: Auto

~~Water levels obtained from Trend Surface Analysis (TSA) Technique can be comparable to measurement at corresponding gauge stations as both follows the same ellipsoid for projection ie WGS 84 and for both measurements, water levels are measured from Mean sea level (M.S. L). As LIDAR DEM is available in Godavari Flood plain, this DEM is taken as reference for calculation of water levels using TSA and FWDET Method. For remaining study areas, COPERNICUS FABDEM is taken as input.~~

The results of the flood water surface derived from surface trend analysis and the Flood Water Depth Estimation Tool (FWDET) indicate that the water surface from the trend analysis closely matches the CWC water surface at gauge stations, whereas the surface derived from the FWDET tool shows significant deviations. ~~Around~~ TSA estimates deviate from ~~a~~ field-level ~~measurements~~ floodwater depth ~~estimation~~measurements by ~~<65cms~~less than 65 cm on ~~an~~ average ~~of~~across 14 gauge stations. Most ~~of~~ interpolated water levels ~~has~~show a small difference ~~(<~~(less than 0.~~5m) with~~5 m) compared to field measurements. The ~~most~~ underestimation of water levels by the TSA method is primarily due to the presence of real-time gauge ~~station~~stations in ~~the~~ upstream flood ~~plain. Similarly~~plains. Conversely, overestimation ~~of water levels is due to presence of~~occurs in areas where gauge ~~station~~stations are located in downstream flood ~~plain. Trend surface methods offer a more balanced and accurate representation of the flood surface in such cases. However, it is observed that slope of the flood affected area plays a major role in flood depth efficiency. For Gentle slope surfaces, the accuracy of this method is better~~plains. ~~Graphs are plotted as per figure~~Trend surface methods provide a more balanced and accurate representation of flood surfaces in such cases. However, it is observed that the slope of the flood-affected area plays a significant role in the accuracy of flood depth estimation. For gentle slopes, the accuracy of the TSA method is notably higher. Graphs are plotted as per fig 10 for the case studies against River gauge station water level and Field measurement, TSA and FWDET methods.

In all ~~the~~ case studies, the Trend Surface Analysis (TSA) method outperforms ~~FwDET~~the FWDET method when ~~compare~~compared to field measurements. The Root Mean Square Error (RMSE) ~~is~~was calculated for ~~these two~~both techniques~~. It is observed~~, with TSA yielding an RMSE ~~for TSA technique is of~~ 0.805, whereas ~~FwDET is~~FWDET produced an RMSE of 5.23. ~~Generally~~FWDET estimates generally exhibit sharp transitions ~~are observed~~ in ~~FwDET estimated~~ flood depth, ~~but here~~while TSA provides ~~the~~a smoother depth distribution ~~of depth map. As the~~. Since TSA-estimated depths ~~from TSA technique~~ also depend on the accuracy of flood extent ~~accuracy, from~~mapping, the ~~above~~ results ~~it is understood~~indicate that

Formatted: English (India)
Formatted: English (India)
Formatted: English (India)
Formatted: English (India)
Formatted: English (India)
Formatted: English (India)
Formatted: English (India)
Formatted: English (India)
Formatted: English (India)
Formatted: English (India)
Formatted: English (India)
Formatted: English (India)
Formatted: English (India)
Formatted: English (India)
Formatted: English (India)
Formatted: English (India)
Formatted: English (India)
Formatted: English (India)
Formatted: English (India)
Formatted: English (India)
Formatted: English (India)
Formatted: English (India)
Formatted: English (India)
Formatted: English (India)
Formatted: English (India)

~~flood mapped output from Automatic Tile~~ the flood maps generated through the automatic tile-based segmentation ~~is seemed~~method appear to be accurate. The ~~entire runtime~~turnaround time for this ~~automated python code ie~~entire process i.e., Flood mapping and Flood depth has ~~took~~taken around 2 min to 5 min depending on the area of case study on a desktop computer 3.2GHz processor and 128 GB RAM

Formatted: English (India)

Formatted: English (India)

Formatted: English (India)

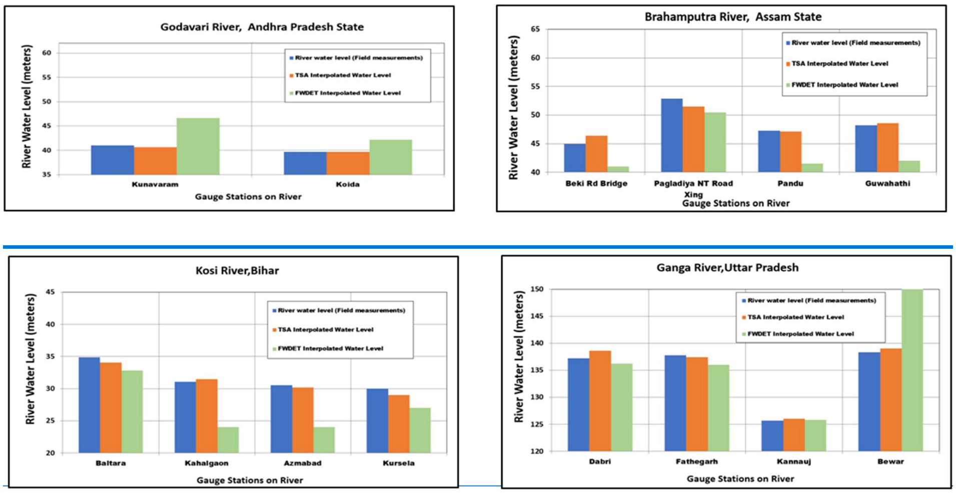

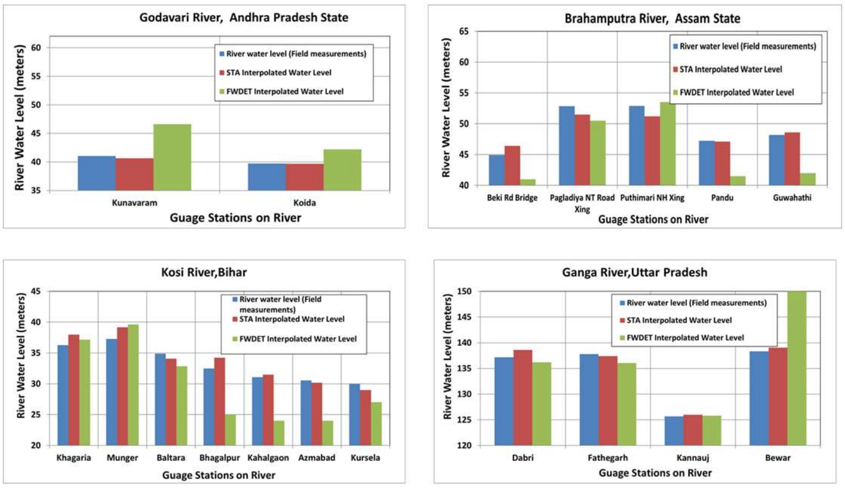

Figure:10 Comparison plots for water levels among field measured data, TSA and FWDET on all study areas

5.3 Discussion

This study introduces a novel approach of frame work for the rapid estimation of flood extent and depth using data from the EOS-04 satellite, marking the first integration of such a methodology. Proposed method enhances the process of deriving flood extent compared to the automatic tile-based threshold technique proposed by Martinis (2015). While the tiling and tile selection criteria remain consistent with the earlier approach, the application of the thresholding technique is a key differentiator. Specifically, we employed the Otsu thresholding method instead of the Kittler and Illingworth minimum error thresholding method. To further improve accuracy, we integrated the Height Above the Nearest Drainage (HAND) tool using Digital Elevation Models (DEMs) to refine flood extent estimations. This enhancement addresses limitations in the earlier technique, offering a more topographically accurate representation of flood extent. Unlike Martinis' reliance on TerraSAR-X data operating in the X band, our approach utilizes data from the EOS-04 satellite, which operates in the C band, demonstrating its applicability to a different radar frequency domain. However, the method has certain limitations like high moisture areas are occasionally misinterpreted as flooded regions due to the radar's sensitivity to water content in soil. Furthermore, the method achieves optimal performance when the entire satellite scene is covered under the tile-fitting framework, ensuring comprehensive data representation.

Trend Surface Analysis (TSA) is classified as a Global Fit interpolation method, which computes a single mathematical function to represent the surface across the flood extent. In contrast, Local Fit methods, such as the Flood Water Depth Estimation Tool (FWDET), estimate surfaces by using nearby data points or reference locations. While Local Fit methods interpolate at discrete points, TSA models the entire surface by leveraging global slope patterns within the data. While FWDET's approach often leads to sharp transitions in depth, TSA produces a smoother distribution of flood depths, effectively capturing overall slope direction and gradients. This makes TSA particularly adept at representing gradual terrain changes and mitigating noise or localized deviations, thereby providing a clearer understanding of flood dynamics over gentle slopes. TSA-derived flood depths were applied to both LiDAR 5m DEM and Copernicus 30m DEM, with results showing a close match in depth estimates for areas with gentle slopes. This demonstrates that even coarser-resolution DEMs, such as the Copernicus 30m DEM, can be effectively utilized for flood depth derivation in regions with gradual terrain changes, thereby broadening the applicability of the method to datasets with varying spatial resolutions.

Despite these advancements, the methodology is highly sensitive to DEM resolution and its alignment with the flood layer. In some cases, manual adjustments are required to ensure proper alignment between the DEM and the corresponding flood extent. Furthermore, while the method performs well in areas with gentle slopes, it faces limitations in steep terrain, where TSA may produce unreliable results. The methodology does not account for hydrodynamic characteristics such as flood velocity or temporal variations in flood behaviour, however, the information generated through the proposed approach is of great help in real time relief and rehabilitation, rescue operations in the field. The rapid and automated nature of the framework makes it suitable for near real-time flood assessment, supporting emergency response efforts. The management decisions, especially during the relief and rehabilitation activities and rescue operations can be made efficiently in terms of deployments of rescue materials like boats/ type boats, and suitably skilled manpower. End-users can confidently use this tool for planning mitigation strategies, such as floodplain zoning and infrastructure protection, while recognizing its constraints in predicting dynamic flood behaviours etc.

6. Conclusions

In summary, the integration of the Automatic Tile~~-~~-Based ~~Classification~~ Segmentation Method ~~applied to EOS-04 data, combined~~ with the HAND (Height Above Nearest Drainage) tool, ~~is~~applied to EOS-04 satellite data, has proven to be a highly effective approach for delineating flood layers~~, particularly in addressing~~. This method addresses key challenges, such as mitigating hill shadows, stray pixels in SAR data to eliminate false water ~~areas. Publicly~~classifications. The study also highlights sensitivity of the using publicly available DEMs~~ are valuable for plain areas~~, such as Copernicus 30m DEM, in regions with gentle slopes where high-resolution DEMs are ~~not available for deriving flood depths, while~~ unavailable. However, for steep flood-prone areas~~ require~~, fine-resolution DEMs ~~for~~remain essential to ensure accurate flood depth estimation.

~~Adopting trend surface methods~~The adoption of Trend Surface Analysis (TSA) for interpolating water ~~levels~~level data ~~allows for more accurate~~further enhances the accuracy and ~~reliable~~reliability of flood depth estimations, particularly in multi-

Formatted: Normal

Formatted: Font: Bold

dimensional river models. ~~These methods capture~~TSA effectively captures the spatial trends inherent in river systems, ~~providing better~~offering improved fitting and~~ more~~ precise representations of flood surfaces~~, especially in rapidly changing conditions. The Global Trend method is particularly effective for generating flood water surfaces in areas with extensive river flooding. This method fits a mathematical surface to the spatial data points, capturing underlying trends and offering a smoother and more accurate representation of the flood surface. By accounting for varying elevations and spatial trends present in the data, the global trend surface approach provides a comprehensive fitting that encompasses the overall spatial trend across the entire study area. This approach is especially useful in large river systems with complex flood behaviours. Combination of~~ . When combined, the Automatic Tile~~ based~~-Based Segmentation ~~technique ~~and TSA ~~technique are proven to be robust, accurate when~~techniques have demonstrated robustness and accuracy, as validated against field-measured data.

~~However, this method is greatly sensitive to DEM resolution and its appropriateness wrt flood layer. Sometimes manual control is required to align the DEM and corresponding flood layer. This method works well only for gentle slope areas. In Steep terrain areas Trend Surface Analysis may behave improperly.~~

Future research will ~~focus on testing this tool on other parts~~aim to test this methodology across diverse regions of the country ~~and try~~to evaluate its broader applicability. Efforts will also focus on refining the approach to ~~improve the methodology based on~~better accommodate varying terrain conditions, including steep slopes, and further improving the alignment and sensitivity of DEM-based flood depth estimations.

Code and data availability

Nil.

Author contributions

Amani and Shashi developed this automated tool. Amani and Suresh tested this tool on field data. Amani, Suresh and Shashi contributed in paper writing. Durga Rao, Srinivas and Prakash technically guided and supported in this automation of Tool.

Competing interests

The authors declare that they have no conflict of interest.

~~References~~

Reference:

Bazi, Y., Bruzzone, L., and Melgani, F.: An unsupervised approach based on the generalized Gaussian model to automatic change detection in multitemporal SAR images, IEEE Trans. Geosci. Remote Sens., 43, 2005.

Boni, G., Ferraris, L., Pulvirenti, L., Squicciarino, G., Pierdicca, N., Candela, L., Pisani, A. R., Zoffoli, S., Onori, R., Proietti, C., and Pagliara, P.: A prototype system for flood monitoring based on flood forecast combined with COSMO-SkyMed and Sentinel-1 data, IEEE J. Sel. Top. Appl. Earth Obs. Remote Sens., 9, 2794–2805, https://doi.org/10.1109/JSTARS.2016.2514402, 2016.

Bovolo, F. and Bruzzone, L.: A split-based approach to unsupervised change detection in large-size multitemporal images: application to tsunami-damage assessment, IEEE Trans. Geosci. Remote Sens., 45, 1658–1670, https://doi.org/10.1109/TGRS.2007.895413, 2007.

Cao, H., Zhang, H., Wang, C., and Zhang, B.: Operational flood detection using Sentinel-1 SAR data over large areas, Water, 11, 786, https://doi.org/10.3390/w11040786, 2019.

Chini, M., Hostache, R., Giustarini, L., and Matgen, P.: A hierarchical split-based approach for parametric thresholding of SAR images: flood inundation as a test case, IEEE Trans. Geosci. Remote Sens., 55, 6975–6988, https://doi.org/10.1109/TGRS.2017.2740462, 2017.

Chini, M., Pelich, R., Pulvirenti, L., Pierdicca, N., Hostache, R., and Matgen, P.: Sentinel-1 InSAR coherence to detect floodwater in urban areas: Houston and Hurricane Harvey as a test case, Remote Sens., 11, 107–120, https://doi.org/10.3390/rs11020107, 2019.

Chorley, R. J., and Haggett, P.: Trend surface mapping in geographical research, Trans. Inst. Br. Geogr., 37, 47–67, https://doi.org/10.2307/621128, 1965.

Cohen, S., Brakenridge, G. R., Kettner, A., Bates, B., Nelson, J. M., McDonald, R. R., Huang, Y.-F., Munasinghe, D., and Zhang, J.: Estimating floodwater depths from flood inundation maps and topography, J. Am. Water Resour. Assoc., 2009.

Cohen, S., Peter, B. G., Haag, A., Munasinghe, D., Moragoda, N., Narayanan, A., and May, S.: Sensitivity of remote sensing floodwater depth calculation to boundary filtering and digital elevation model selections, Am. Water Resour. Assoc., 2022.

Costabile, P., Costanzo, C., Ferraro, D., and Barca, P.: Is HEC-RAS 2D accurate enough for storm-event hazard assessment? Lessons learnt from a benchmarking study based on rain-on-grid modelling, J. Hydrol., 2021.

Elkhrachy, I.: Flash flood water depth estimation using SAR images, digital elevation models, and machine learning algorithms, Remote Sens., 14, 440, https://doi.org/10.3390/rs14030440, 2022.

Giacomelli, A., Mancini, M., and Rosso, R.: Assessment of flooded areas from ERS-1 PRI data: an application to the 1994 flood in Northern Italy, Phys. Chem. Earth, 20, 469–474, https://doi.org/10.1016/S0079-1946(96)00009-6, 1995.

Giustarini, L., Hostache, R., and D.K.O., G.: Probabilistic flood mapping using synthetic aperture radar data, IEEE Trans. Geosci. Remote Sens., 54, 6958–6969, https://doi.org/10.1109/TGRS.2016.2592951, 2016.

Greifeneder, F., Wagner, W., Sabel, D., and Naeimi, V.: Suitability of SAR imagery for automatic flood mapping in the Lower Mekong Basin, Int. J. Remote Sens., 35, 2857–2874, https://doi.org/10.1080/01431161.2014.880829, 2014.

Horritt, M. S., Mason, D. C., and Luckman, A. J.: Flood boundary delineation from Synthetic Aperture Radar imagery using a statistical active contour model, Int. J. Remote Sens., 22, 2489–2507, 2001.

Islam, M. M., and Sadu, K.: Flood damage and modelling using satellite remote sensing data with GIS: Case study of Bangladesh, in: Remote Sensing and Hydrology 2000, IAHS Publication, edited by: Owe, M., Brubaker, K., Ritchie, J., and Rango, A., Oxford, UK, 455–458, 2001.

Joshi, A., Agrawal, S., and Singh, R. P.: Potential of EOS-4 imagery for SAR interferometry, Remote Sens. Appl. Soc. Environ., 32, 101010, https://doi.org/10.1016/j.rsase.2023.101010, 2023.

Kittler, J., and Illingworth, J.: Minimum error thresholding, Pattern Recognit., 19, 41–47, https://doi.org/10.1016/0031-3203(86)90030-0, 1986.

Kuenzer, C., Guo, H., Schlegel, I., Tuan, V., Li, X., and Dech, S.: Varying scale and capability of Envisat ASAR-WSM, TerraSAR-X Scansar and TerraSAR-X Stripmap data to assess urban flood situations: a case study of the Mekong delta in Can Tho province, Remote Sens., 5, 5122–5142, https://doi.org/10.3390/rs5105122, 2013.

Lam, N. S.-N.: Spatial interpolation methods: a review, The Am. Cartogr., March 2013.

Li, N., Wang, R., Liu, Y., Du, K., Chen, J., and Deng, Y.: Robust river boundaries extraction of dammed lakes in mountain areas after Wenchuan Earthquake from high-resolution SAR images combining local connectivity and ACM, ISPRS J. Photogramm. Remote Sens., 94, 91–101, 2014.

Manjusree, P., Kumar, L. P., Bhatt, C. M., Rao, G. S., and Bhanumurthy, V.: Optimization of threshold ranges for rapid flood inundation mapping by evaluating backscatter profiles of high incidence angle SAR images, Int. J. Disaster Risk Sci., 3, 113–122, 2012.

Mason, D. C., Giustarini, L., Garcia-Pintado, J., and Cloke, H. L.: Detection of flooded urban areas in high-resolution synthetic aperture radar images using double scattering, Int. J. Appl. Earth Obs. Geoinf., 28, 150–159, https://doi.org/10.1016/j.jag.2013.12.002, 2014.

Mason, D. C., Speck, R., Devereux, B., Schumann, G. J. P., Neal, J. C., and Bates, P. D.: Flood detection in urban areas using TerraSAR-X, IEEE Trans. Geosci. Remote Sens., 48, 2010.

Marti-Cardona, B., Dolz-Ripolles, J., and Lopez-Martinez, C.: Wetland inundation monitoring by the synergistic use of ENVISAT/ASAR imagery and ancillary spatial data, Remote Sens. Environ., 139, 171–184, https://doi.org/10.1016/j.rse.2013.08.020, 2013.

Martinis, S., Kersten, J., and Twele, A.: A fully automated TerraSAR-X based flood service, ISPRS J. Photogramm. Remote Sens., 104, 203–212, https://doi.org/10.1016/j.isprsjprs.2014.07.014, 2015.

Martinis, S., Twele, A., Strobl, C., Kersten, J., and Stein, E.: A multi-scale flood monitoring system based on fully automatic MODIS and TerraSAR-X processing chains, Remote Sens., 5, 5598–5619, 2013.

Mazzarino, M., and Bonifazi, A.: A new approach to flood mapping from SAR images based on the analysis of water-to-land transitions, Int. J. Remote Sens., 39, 2233–2255, https://doi.org/10.1080/01431161.2017.1415867, 2018.

Mehr, A. J., Nejadkoorki, F., and Makhdoum, M. M.: Assessing the capabilities of C-band SAR data for flood mapping: a case study of the 2010 floods in Pakistan, Remote Sens. Environ., 119, 238–247, https://doi.org/10.1016/j.rse.2011.12.013, 2012.

Nemani, R. R., and Running, S. W.: Estimation of global land surface evaporation using satellite data, J. Appl. Meteorol. Climatol., 34, 1395–1409, 1995.

Nuth, C., and Kääb, A.: Two decades of multiview stereo topographic mapping of the Earth's surface, Remote Sens. Environ., 169, 54–65, https://doi.org/10.1016/j.rse.2015.08.023, 2015.

Pender, G., and Chanson, H.: The analysis of high-resolution floodplain inundation and flood risk using a remote sensing approach, Water, 10, 163, https://doi.org/10.3390/w10020163, 2018.

Perciavalle, V., Bagnato, S., and Lupo, D.: The use of SAR images for flood monitoring in Sicilian coastal areas: first results of an experimental study, Remote Sens., 12, 1536, https://doi.org/10.3390/rs12091536, 2020.

Platt, S. R., and Tazik, D. J.: Use of remote sensing in flood prediction: lessons from the 1998 flooding of the Red River in North Dakota and Minnesota, Water Resour. Bull., 34, 289–300, 1998.

Pulselli, F. M., and Salata, F.: Flood inundation mapping from optical remote sensing images and its operational integration with local emergency management protocols, Nat. Hazards Earth Syst. Sci., 16, 1357–1372, https://doi.org/10.5194/nhess-16-1357-2016, 2016.

Schumann, G., Bates, P. D., Horritt, M. S., Matgen, P., and Pappenberger, F.: Progress in integration of remote sensing–derived flood extent and stage data and hydraulic models, Rev. Geophys., 47, https://doi.org/10.1029/2008RG000274, 2009.

Scolobig, A., and Petrucci, O.: The role of imagery in building flood resilience: a case study from the 2014 flood in the Emilia-Romagna region, Italy, Nat. Hazards Earth Syst. Sci., 16, 1549–1563, https://doi.org/10.5194/nhess-16-1549-2016, 2016.

Stewart, C., and Arnold, M.: Flood risk assessment and management in a changing climate: new approaches and solutions, Water, 11, 56, https://doi.org/10.3390/w11010056, 2019.

Tabrizi, S. J. and Rahimi, M. M.: A novel model for flood mapping using multispectral remote sensing images, Remote Sens., 13, 2120, https://doi.org/10.3390/rs13122120, 2021.

Van Zyl, J. J., and Jezek, K. C.: A remote sensing approach to flood assessment and mapping, Remote Sens. Environ., 119, 134–147, https://doi.org/10.1016/j.rse.2011.02.012, 2012.

Voigt, S., and Rinnert, E.: A concept for rapid flood mapping using synthetic aperture radar data based on the normalised water index, Remote Sens., 10, 1037, https://doi.org/10.3390/rs10071037, 2018.

Wong, H. K., Chan, T. O., and Cheung, M. K.: Real-time flood monitoring system based on near real-time data acquisition and satellite remote sensing, IEEE J. Sel. Top. Appl. Earth Obs. Remote Sens., 9, 1320–1329, https://doi.org/10.1109/JSTARS.2016.2530861, 2016.

Xu, H., and Lin, H.: Use of SAR data for urban flood mapping, Remote Sens. Environ., 143, 147–160, https://doi.org/10.1016/j.rse.2013.02.013, 2013.